

Solid-state
physics

P7 Solid-state physics

P 7.1 Properties of crystals

P 7.1.1	Structure of crystals	237
P 7.1.2	X-ray structural analysis	238
P 7.1.3	X-ray structural analysis with the x-ray apparatus P	239
P 7.1.4	Elastic and plastic deformation	240

P 7.2 Conduction phenomena

P 7.2.1	Hall effect	241
P 7.2.2	Electrical conduction in solid bodies	242
P 7.2.3	Photoconductivity	243
P 7.2.4	Luminescence	244
P 7.2.5	Thermoelectricity	245
P 7.2.6	Superconductivity	246

P 7.3 Magnetism

P 7.3.1	Dia-, para- und ferromagnetism	247
P 7.3.2	Ferromagnetic hysteresis	248

P 7.4 Scanning probe microscopy

P 7.4.1	Scanning tunneling microscope	249
---------	-------------------------------	-----



Investigating the crystal structures of tungsten using a field emission microscope (P 7.1.1.1)

P 7.1.1

Structure of crystals

P 7.1.1.1 Investigating the crystal structures of tungsten using a field emission microscope

Cat. No.	Description	P 7.1.1.1
554 60	Field emission microscope	1
554 605	Connection plate FEM	1
301 339	Pair of stand feet	1
521 70	High voltage power supply 10 kV	1
521 39	Variable extra low voltage transformer	1
531 130	Ammeter, DC, $I \leq 10$ A, e. g. Multimeter Danalog 30	1
500 614	Safety connection lead, 25 cm, black	2
500 624	Safety connection lead, 50 cm, black	2
500 641	Safety connection lead, 100 cm, red	1
500 642	Safety connection lead, 100 cm, blue	1
500 644	Safety connection lead, 100 cm, black	2

In the field emission microscope, the extremely fine tip of a tungsten monocrystal is arranged in the center of a spherical luminescent screen. In the vicinity of the tip, the electric field between the crystal and the luminescent screen reaches such a high field strength that the conducting electrons can “tunnel” out of the crystal and travel radially to the luminescent screen. Here, an image of the emission distribution of the crystal tip is created, magnified by a factor of

$$V = \frac{R}{r}$$

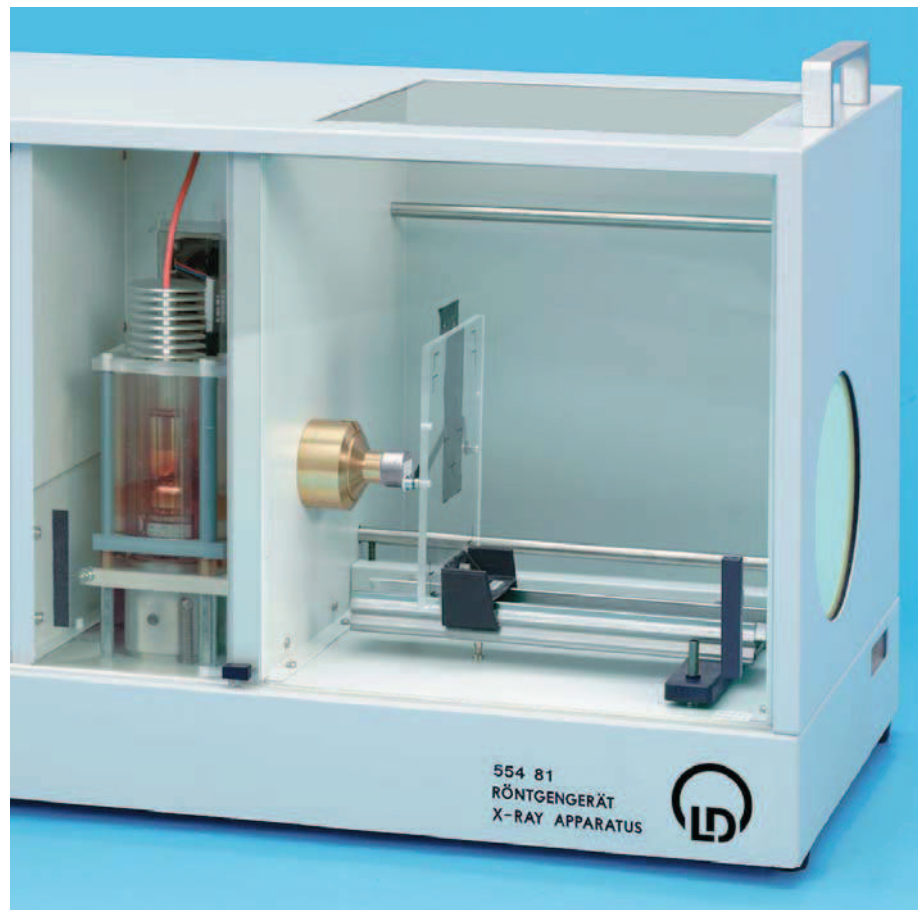
$R = 5$ cm: radius of luminescent screen
 $r = 0,1\text{--}0,2$ μm : radius of tip

In the first part of this experiment, the tungsten tip is purified by heating it to a white glow. The structure which appears on the luminescent screen after the electric field is applied corresponds to the body-centered cubic lattice of tungsten, which is observed in the (110) direction, i.e. the direction of one of the diagonals of a cube face. Finally, a minute quantity of barium is vaporized in the tube, so that individual barium atoms can precipitate on the tungsten tip to produce bright spots on the luminescent screen. When the tungsten tip is heated carefully, it is even possible to observe the thermal motion of the barium atoms.

P 7.1.2

X-ray structural analysis

- P 7.1.2.1 Bragg reflection:
determining the lattice constants
of monocrystals
- P 7.1.2.2 Laue diagrams:
investigating the lattice structure
of monocrystals
- P 7.1.2.3 Debye-Scherrer photography:
determining the lattice-plane
spacings of polycrystalline
powder samples
- P 7.1.2.4 Debye-Scherrer Scan:
determining the lattice-plane
spacings of polycrystalline
powder samples



Laue diagrams: investigating the lattice structure of monocrystals (P 7.1.2.2)

When x-rays of the wavelength λ are diffracted at a crystal, maxima occur at the reflection angles α , β , γ which, when measured with respect to the crystal axes a , b , c , fulfill the Laue conditions

$$h \cdot \lambda = a \cdot (\cos \alpha_0 - \cos \alpha), h = 0, \pm 1, \pm 2, \dots$$

$$k \cdot \lambda = b \cdot (\cos \beta_0 - \cos \beta), k = 0, \pm 1, \pm 2, \dots$$

$$l \cdot \lambda = c \cdot (\cos \gamma_0 - \cos \gamma), l = 0, \pm 1, \pm 2, \dots$$

α_0 , β_0 , γ_0 : angle of incidence

W. H. and W. L. Bragg described the behavior of x-rays in crystals in simplified terms as reflection at a set of parallel lattice planes. Reflection can only occur for the glancing angles ϑ which fulfill the Bragg condition

$$2 \cdot d \cdot \sin \vartheta = n \cdot \lambda \text{ with } n = 1, 2, 3, \dots$$

d : lattice plane spacing, n : diffraction order

For a cubic lattice with the lattice constant a , the spacing of the lattice planes can be expressed using the Laue indices h , k , l :

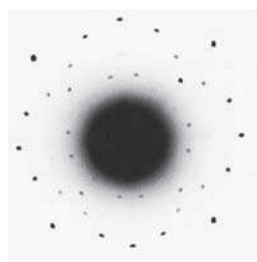
$$d = \frac{a}{\sqrt{h^2 + k^2 + l^2}}$$

In the first experiment, the Bragg reflection of Mo- K_α radiation ($\lambda = 71.080$ pm) at NaCl and LiF monocrystals is used to determine the lattice constant. The K_β component of the x-ray radiation can be suppressed using a zirconium filter.

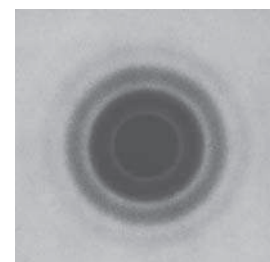
To make Laue diagrams at NaCl and LiF monocrystals, the bremsstrahlung radiation of the x-ray apparatus is used in the second experiment as "white" x-radiation. The positions of the "colored" reflections on an x-ray film behind the crystal and their intensities can be used to determine the crystal structure and the lengths of the crystal axes through application of the Laue condition.

In the last two experiments, Debye-Scherrer photographs are produced by irradiating samples of a fine crystal powder with Mo- K_α radiation. Among many unordered crystallites of the sample, the x-rays diffract at those which have an orientation conforming to the Bragg condition. The diffracted rays describe conical sections for which the aperture angles ϑ can be derived

Cat. No.	Description	P 7.1.2.1	P 7.1.2.2	P 7.1.2.3	P 7.1.2.4
554 811USB	X-ray apparatus	1	1	1	1
559 01	End-window counter for a, b, g and x-rays	1			1
554 77	LiF monocrystal for Bragg reflection	1			
554 842	Set of 2 crystal powder-holder				1
554 838	Film holder x-ray		1	1	
554 896	X-ray film Agfa Dentus M2		1	1	
554 897	Developer for X-ray film		1	1	
554 898	Fixative for X-ray film		1	1	
554 899	Development tank 500 ml		1*	1*	
554 899	Changing bag for the development tank		1*	1*	
554 87	LiF crystal for Laue diagrams		1		
554 88	NaCl crystal for Laue diagrams		1		
667 091	Pestle, porcelain, 100 mm, for 667 092			1	1
667 092	Mortar, porcelain, 63 mm dia.			1	1
311 54	Precision vernier calipers			1	
	additionally required: PC with Windows 95/98/NT or higher	1			1



Laue diagram of NaCl



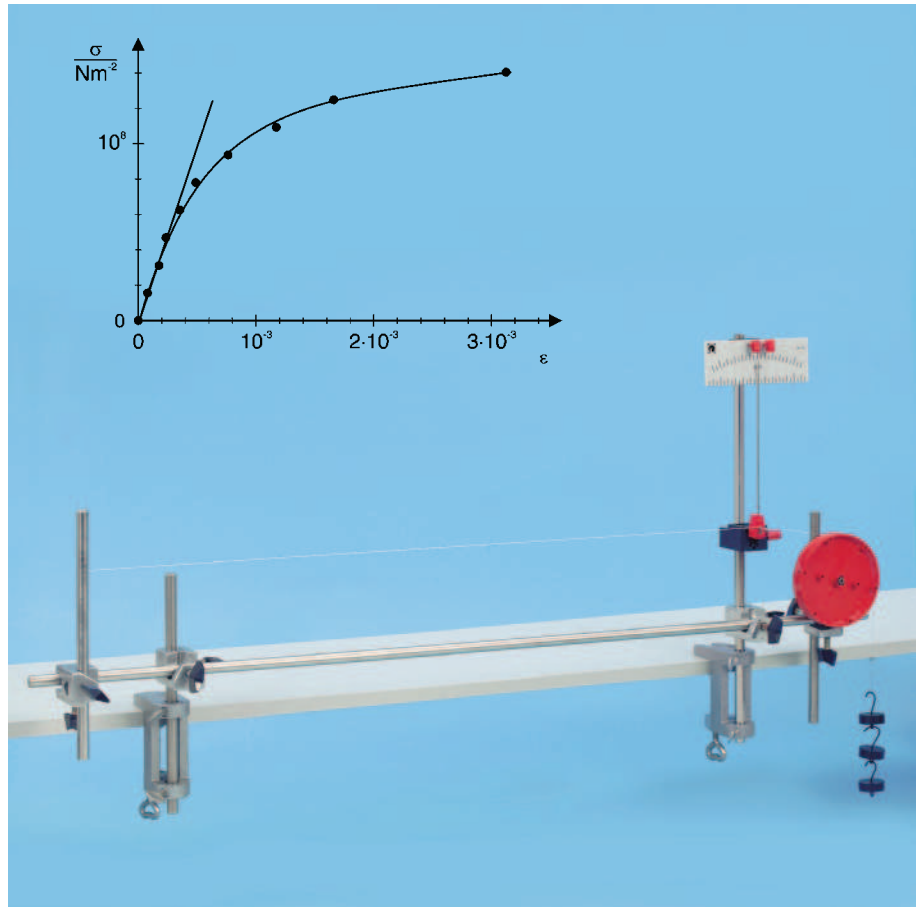
Debye-Scherrer photograph of NaCl

from a photograph. This experiment determines the lattice spacing corresponding to ϑ as well as its Laue indices h , k , l , and thus the lattice structure of the crystallite.

P 7.1.4

Elastic and plastic deformation

P 7.1.4.1 Investigating the elastic and plastic extension of metal wires



Investigating the elastic and plastic extension of copper wires (P 7.1.4.1)

The shape of a crystalline solid is altered when a force is applied. We speak of elastic behavior when the solid resumes its original form once the force ceases to act on it. When the force exceeds the elastic limit, the body is permanently deformed. This plastic behavior is caused by the migration of discontinuities in the crystal structure.

In this experiment, the extension of iron and copper wires is investigated by hanging weights from them. A precision pointer indicator measures the change in length Δs , i.e. the extension

$$\varepsilon = \frac{\Delta s}{s}$$

s : length of wire

After each new tensile load

$$\sigma = \frac{F}{A}$$

F : weight of load pieces,
 A : wire cross-section

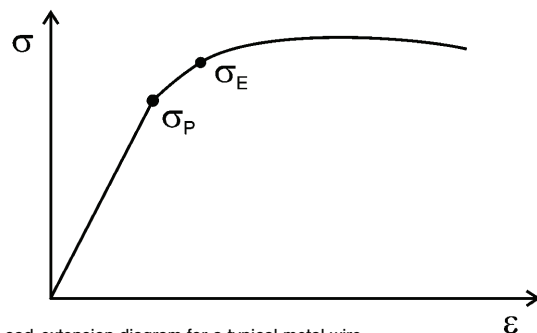
the students observe whether the pointer returns to the zero position when the strain is relieved, i.e. whether the strain is below the elasticity limit σ_E . Graphing the measured values in a tension-extension diagram confirms the validity of Hooke's law

$$\sigma = E \cdot \varepsilon$$

E : modulus of elasticity

up to a proportionality limit σ_P .

Cat. No.	Description	P 7.1.4.1
550 35	Copper wire, 100 m, 0.20 mm dia.	1
550 51	Iron wire, 100 m, 0.20 mm dia.	1
342 61	Set of 12 weights, 50 g each	2
340 911	Pulley, plug-in, 50 mm diameter	1
381 331	Pointer for linear expansion	1
340 82	Double scale	1
314 04	Support clip, for plugging in	2
301 07	Simple bench clamp	2
301 01	Leybold multiclamp	4
301 25	Clamping block MF	3
301 26	Stand rod, 25 cm, 10 mm dia.	3
301 27	Stand rod, 50 cm, 10 mm dia.	1
300 44	Stand rod, 100 cm	1



Load-extension diagram for a typical metal wire



Investigating the Hall effect in silver (P 7.2.1.1)(a)

P 7.2.1

Hall effect

P 7.2.1.1 Investigating the Hall effect in silver

P 7.2.1.2 Investigating the anomalous Hall effect in tungsten

P 7.2.1.3 Determining the density and mobility of charge carriers in n-germanium
CASSY-SP 7.2.1.4 Determining the density and mobility of charge carriers in p-germanium
CASSY-SP 7.2.1.5 Determining the band gap of germanium
CASSY-S

Cat. No.	Description	P 7.2.1.1(a)	P 7.2.1.1(b)	P 7.2.1.2(a)	P 7.2.1.2(b)	P 7.2.1.3	P 7.2.1.4	P 7.2.1.5
586 81	Hall effect apparatus, silver	1	1					
586 84	Hall effect apparatus, tungsten			1	1			
586 850	Base unit for Hall effect (Ge)					1	1	1
586 853	n-Ge on plug-in board					1		
586 852	p-Ge on plug-in board						1	
586 851	Ge undoped on plug-in board							1
532 13	Microvoltmeter	1	1					
531 835	Universal Measuring Instrument Physics	1	1					
524 009	Mobile-CASSY	2		2				
524 040	μV-box	1		1				
524 010USB	Sensor CASSY					1	1	1
524 200	CASSY Lab					1	1	1
524 0381	Combi B-sensor S	1	1	1	1	1	1	
501 11	Extension cable, 15-pole	1	1	1	1	1	1	
521 55	High current power supply	1	1	1	1			
521 39	Variable extra low voltage transformer	1	1	1	1			
521 501	AC/DC power supply 0....15 V					2	2	1
521 545	DC power supply 0....16 V, 5 A					1	1	1
562 11	U-core with yoke	1	1	1	1	1	1	
560 31	Pair of bored pole pieces	1	1	1	1	1	1	
562 13	Coil with 250 turns	2	2	2	2	2	2	
531 130	Multimeter LD analog 30	1	1	1	1			
300 41	Stand rod, 25 cm	1	1	1	1	1	1	
301 01	Leybold multiclamp	1	1	1	1	1	1	
300 02	Stand base, V-shape, 20 cm	1	1	1	1	1	1	1
501 46	Pair of cables, 1 m, red and blue	4	4	4	4	7	7	4
501 33	Connecting lead, Ø 2.5 mm2, 100 cm, black	2	2	2	2			
additionally required:								
PC with Windows 95/98/NT or higher						1	1	1

In the case of electrical conductors or semiconductors within a magnetic field B , through which a current I is flowing perpendicular to the magnetic field, the Hall effect results in an electric potential difference

$$U_H = R_H \cdot B \cdot I \cdot \frac{1}{d}$$

d : thickness of sample

The Hall coefficient

$$R_H = \frac{1}{e} \cdot \frac{p \cdot \mu_p^2 - n \cdot \mu_n^2}{(p \cdot \mu_p + n \cdot \mu_n)^2}$$

e : elementary charge

depends on the concentrations n and p of the electrons and holes as well as their mobilities μ_n and μ_p , and is thus a quantity which depends on the material and the temperature.

The first two experiments determine the Hall coefficient R_H of two electrical conductors by measuring the Hall voltage U_H for various currents I as a function of the magnetic field B . A negative value is obtained for the Hall coefficient of silver, which indicates that the charge is being transported by electrons. A positive value is found as the Hall coefficient of tungsten. Consequently, the holes are mainly responsible for conduction in this metal.

The third and fourth experiments explore the temperature-dependency of the Hall voltage and the electrical conductivity

$$\sigma = e \cdot (p \cdot \mu_p + n \cdot \mu_n)$$

using doped germanium samples. The concentrations of the charge carriers and their mobilities are determined under the assumption that, depending on the doping, one of the concentrations n or p can be ignored. In the final experiment, the electrical conductivity of undoped germanium is measured as a function of the temperature to provide a comparison. The measurement data permits determination of the band gap between the valence band and the conduction band in germanium.

P 7.2.2

Electrical conduction in solid bodies

- P 7.2.2.1

CASSY-S

Measuring the temperature-dependency of a noble metal resistor
- P 7.2.2.2

CASSY-S

Measuring the temperature-dependency of a semiconductor resistor



Measuring the temperature-dependency of a noble metal resistor and a semiconductor resistor (P 7.2.2.1/2)

The temperature-dependency of the specific resistance ρ is a simple test for models of electric conductivity of conductors and semiconductors. In electrical conductors, ρ increases with the temperature, as the collisions of the quasi-free electrons from the conduction band with the atoms of the conductor play an increasingly important role. In semiconductors, on the other hand, the specific resistance decreases as the temperature increases, as more and more electrons move from the valence band to the conduction band, thus contributing to the conductivity.

These experiments measure the resistance values as a function of temperature using a Wheatstone bridge. The computer-assisted CASSY measured-value recording system is ideal for recording and evaluating the measurements. For the noble metal resistor, the relationship

$$R = R_{\Theta} \cdot \frac{T}{\Theta}$$

$\Theta = 240 \text{ K: Debye temperature of platinum}$

is verified with sufficient accuracy in the temperature range under study. For the semiconductor resistor, the evaluation reveals a dependency with the form

$$R \propto e^{-\frac{\Delta E}{2kT}}$$

$k = 1.38 \cdot 10^{-23} \frac{\text{J}}{\text{K}}$: Boltzmann constant

with the band spacing $E = 0.48 \text{ eV}$.

Cat. No.	Description	P 7.2.2.1	P 7.2.2.2
586 80	Noble metal resistor	1	
586 82	Semiconductor resistor		1
555 81	Electric oven for 230 V	1	1
524 031	Current supply box	1	1
529 676	NiCr-Ni temperature sensor 1.3 mm	1	1
524 0673	NiCr-Ni adapter S	1	1
524 010USB	Sensor-CASSY	1	1
524 200	CASSY Lab	1	1
502 061	Safety connection box with ground	1	1
501 45	Pair of cables, 50 cm, red and blue	1	1
	additionally required: PC with Windows 95/98/NT or higher	1	1



P 7.2.3

Photoconductivity

P 7.2.3.1 Recording the current-voltage characteristic of a CdS photoresistor



Recording the current-voltage characteristic of a CdS photoresistor (P 7.2.3.1)

Cat. No.	Description	P 7.2.3.1
578 02	STE photoresistor LDR 05	1
460 21	Holder for plug-in elements	1
450 60	Lamp housing	1
450 51	Lamp, 6 V/30 W	1
521 210	Transformer, 6 V AC, 12 V AC/30 VA	1
460 20	Aspherical condensor	1
472 401	Polarization filter	2
460 08	Lens $f = +150$ mm	1
460 32	Precision optical bench, standardized cross section 1 m	1
460 374	Optics rider, $H = 90$ mm/ $W = 50$ mm	6
460 14	Adjustable slit	1
521 545	DC power supply 0...16 V, 5 A	1
531 281	Digital-analog multimeter METRAHit 24 S	1
531 301	Digital-analog multimeter METRAHit 26 S	1
500 422	Connecting lead, 50 cm, blue	1
501 46	Pair of cables, 100 cm, red and blue	2

Photoconductivity is the phenomenon in which the electrical conductivity σ of a solid is increased through the absorption of light. In CdS, for example, the absorbed energy enables the transition of activator electrons to the conduction band and the reversal of the charges of traps, with the formation of electron holes in the valence band. When a voltage U is applied, a photocurrent I_{ph} flows.

The object of the experiment is to determine the relationship between the photocurrent I_{ph} and the voltage U at a constant radiant flux Φ_e as well as between the photocurrent I_{ph} and the radiant flux Φ_e at a constant voltage U in the CdS photoresistor.

P 7.2.4

Luminescence

P 7.2.4.1 Exciting luminescence through irradiation with ultraviolet light and electrons



Exciting luminescence through irradiation with ultraviolet light and electrons (P 7.2.4.1)

Luminescence is the emission of light following the absorption of energy. This energy can be transmitted in the form of e.g. high-energy electrons or photons which have an energy greater than that of the emitted photons. Depending on the type of decay, we distinguish between fluorescence and phosphorescence. In fluorescence, the emission of photons fades exponentially very rapidly when excitation is switched off (i.e. about 10^{-8} s). Phosphorescence, on the other hand, can persist for several hours. In this experiment, the luminescence of various solids following irradiation with ultraviolet light or electrons is demonstrated. These samples include yttrium vanadate doped with europium (red fluorescent), zinc silicate doped with manganese (green fluorescent) and barium magnesium aluminate doped with europium (blue fluorescent).

Note: It is possible to recognize individual emission lines within the band spectrum using a pocket spectroscope.

Cat. No.	Description	P 7.2.4.1
555 618	Luminescent tube	1
555 600	Stand for electron tubes	1
521 70	High voltage power supply 10 kV	1
451 15	High-pressure mercury lamp	1
451 19	Lamp socket E27 on rod for high-pressure mercury lamp	1
451 30	Universal choke 230 V, 50 Hz	1
469 79	Ultraviolet filter	1
300 11	Saddle base	1
500 611	Safety connecting lead, 25 cm, red	1
500 621	Safety connecting lead, 50 cm, red	1
500 641	Safety connecting lead, 100 cm, red	1
500 642	Safety connecting lead, 100 cm, blue	1
500 644	Safety connecting lead, 100 cm, black	2





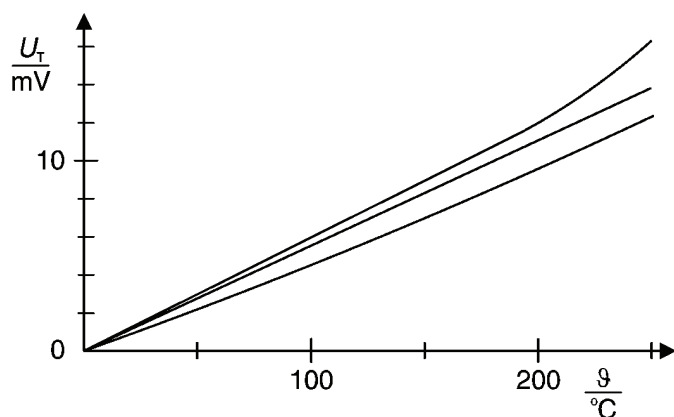
P 7.2.5

Thermoelectricity

P 7.2.5.1 Seebeck effect:
Determining the thermoelectric
voltage as a function of the
temperature differential

Seebeck effect: Determining the thermoelectric voltage as a function of the temperature differential (P 7.2.5.1)

Cat. No.	Description
557 01	Set of 3 simple thermocouples
590 011	Clamping plug
532 13	Microvoltmeter
382 34	Thermometer, -10° to + 110 °C
666 767	Hot plate, 150 mm dia., 1500 W
664 104	Beaker, 400 ml, ss, hard glass
524 009	Mobile-CASSY
524 040	µV-box



Thermoelectric voltage as a function of the temperature
Top: chrome-nickel/constantan, Middle: iron/constantan, Bottom: copper/constantan

P 7.2.5.1 (a)
1 1
2 2
1 1
1 1
1 1
1 1
1 1

When two metal wires with different Fermi energies E_F touch, electrons move from one to the other. The metal with the lower electronic work function W_A emits electrons and becomes positive. The transfer does not stop until the contact voltage

$$U = \frac{W_{A,1} - W_{A,2}}{e}$$

e : elementary charge

is reached. If the wires are brought together in such a way that they touch at both ends, and if the two contact points have a temperature differential $T = T_1 - T_2$, an electrical potential, the thermoelectric voltage

$$U_T = U(T_1) - U(T_2),$$

is generated. Here, the differential thermoelectric voltage

$$\alpha = \frac{dU_T}{dT}$$

depends on the combination of the two metals.

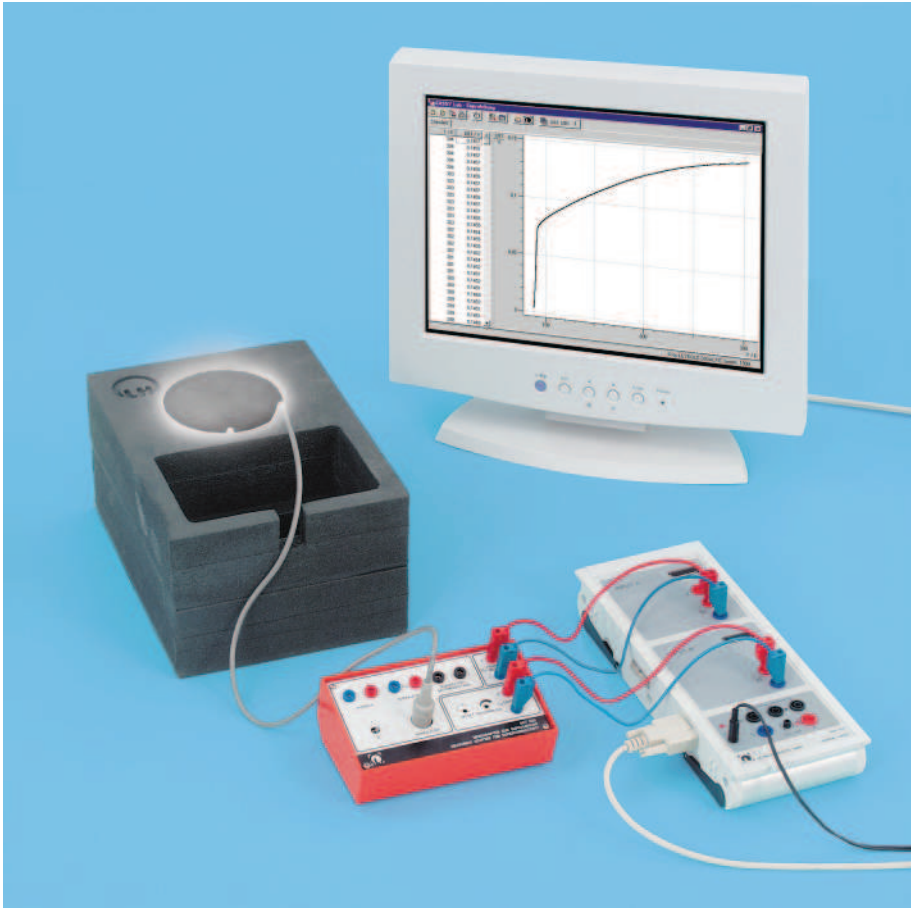
In this experiment, the thermoelectric voltage U_T is measured as a function of the temperature differential T between the two contact points for thermocouples with the combinations iron/constantan, copper/constantan and chrome-nickel/constantan. One contact point is continuously maintained at room temperature, while the other is heated in a water bath. The differential thermoelectric voltage is determined by applying a best-fit straight line

$$U_T = \alpha \cdot T$$

to the measured values.

P 7.2.6
Superconductivity

- P 7.2.6.1 **CASSY-S** Determining the transition temperature of a high-temperature superconductor
- P 7.2.6.2 Meißner-Ochsenfeld effect in a high-temperature superconductor



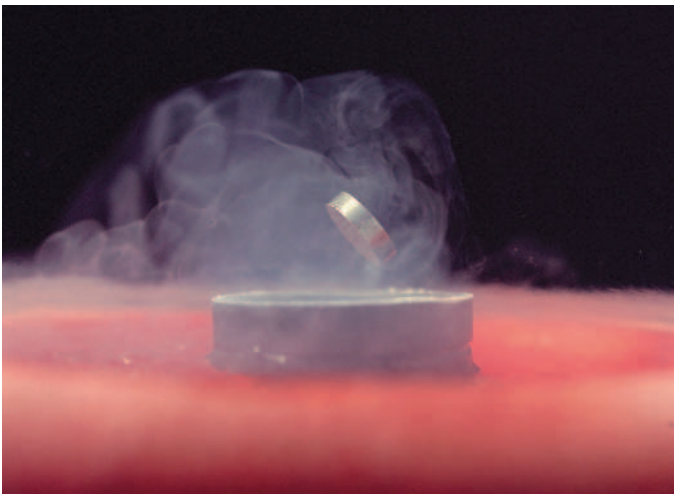
Determining the transition temperature of a high-temperature superconductor (P 7.2.6.1)

In 1986, K. A. Müller and J. G. Bednorz succeeded in demonstrating that the compound $\text{YBa}_2\text{Cu}_3\text{O}_7$ becomes superconducting at temperatures far greater than any known up to that time. Since then, many high-temperature superconductors have been found which can be cooled to their transition temperature using liquid nitrogen. Like all superconductors, high-temperature superconductors have no electrical resistance and demonstrate the phenomenon known as the Meissner-Ochsenfeld effect, in which magnetic fields are displaced out of the superconducting body.

The first experiment determines the transition temperature of the high-temperature superconductor $\text{YBa}_2\text{Cu}_3\text{O}_{7-x}$. For this purpose, the substance is cooled to below its critical temperature of $T_c = 92 \text{ K}$ using liquid nitrogen. In a four-point measurement setup, the voltage drop across the sample is measured as a function of the sample temperature using the computer-assisted measured value recording system CASSY.

In the second experiment, the superconductivity of the $\text{YBa}_2\text{Cu}_3\text{O}_{7-x}$ body is verified with the aid of the Meissner-Ochsenfeld effect. A low-weight, high field-strength magnet placed on top of the sample begins to hover when the sample is cooled to below its critical temperature so that it becomes superconducting and displaces the magnetic field of the permanent magnet.

Cat. No.	Description	P 7.2.6.1	P 7.2.6.2
667 552	Experiment kit for determining transition temperature and electrical resistance	1	
524 010USB	Sensor-CASSY	1	
524 200	CASSY Lab	1	
501 45	Pair of cables, 50 cm, red and blue	2	
667 551	Experiment kit for Meissner-Ochsenfeld effect		1
	additionally required: PC with Windows 95/NT or higher	1	



Meißner-Ochsenfeld effect in a high-temperature superconductor



P 7.3.1

Dia-, para- and ferromagnetism

P 7.3.1.1 Dia-, para- and ferromagnetic materials in an inhomogeneous magnetic field

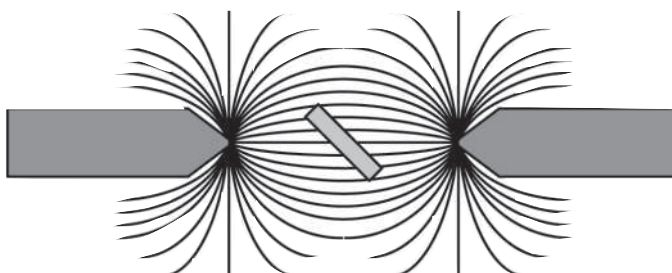


Dia-, para- and ferromagnetic materials in an inhomogeneous magnetic field (P 7.3.1.1)

Cat. No.	Description	P 7.3.1.1
560 41	Apparatus for experiments on dia- and paramagnetism	1
562 11	U-core with yoke	1
562 13	Coil with 250 turns	2
560 31	Pair of bored pole pieces	1
521 39	Variable extra low voltage transformer	1
300 02	Stand base, V-shape, 20 cm	1
300 41	Stand rod, 25 cm	2
301 01	Leybold multiclamp	1
501 46	Pair of cables, 100 cm, red and blue	1
500 422	Connecting lead, 50 cm, blue	1

Diamagnetism is the phenomenon in which an external magnetic field causes magnetization in a substance which is opposed to the applied magnetic field in accordance with Lenz's law. Thus, in an inhomogeneous magnetic field, a force acts on diamagnetic substances in the direction of decreasing magnetic field strength. Paramagnetic materials have permanent magnetic moments which are aligned by an external magnetic field. Magnetization occurs in the direction of the external field, so that these substances are attracted in the direction of increasing magnetic field strength. Ferromagnetic substances in magnetic fields assume a very high magnetization which is orders of magnitude greater than that of paramagnetic substances.

In this experiment, three 9 mm long rods with different magnetic behaviors are suspended in a strongly inhomogeneous magnetic field so that they can easily rotate, allowing them to be attracted or repelled by the magnetic field depending on their respective magnetic property.

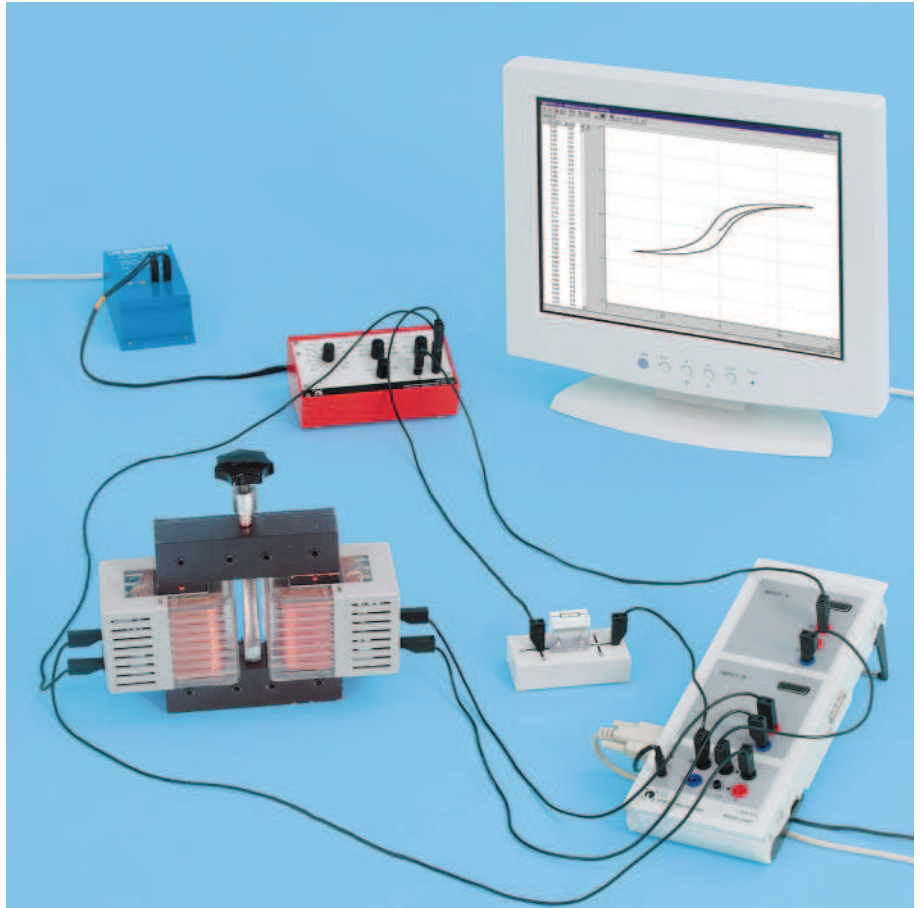


Placement of a sample in the magnetic field

P 7.3.2

Ferromagnetic hysteresis

P 7.3.2.1 Recording the magnetization and hysteresis curves of a ferromagnet



Recording the magnetization and hysteresis curves of a ferromagnet (P 7.3.2.1 a)

In a ferromagnet, the magnetic induction

$$B = \mu_r \cdot \mu_0 \cdot H$$

$$\mu_0 = 4\pi \cdot 10^{-7} \frac{\text{Vs}}{\text{Am}}: \text{magnetic field constant}$$

reaches a saturation value B_s as the magnetic field H increases. The relative permeability μ_r of the ferromagnet depends on the magnetic field strength H , and also on the previous magnetic treatment of the ferromagnet. Thus, it is common to represent the magnetic induction B in the form of a hysteresis curve as a function of the rising and falling field strength H . The hysteresis curve differs from the magnetization curve, which begins at the origin of the coordinate system and can only be measured for completely demagnetized material.

In this experiment, a current I_1 in the primary coil of a transformer which increases (or decreases) linearly over time generates the magnetic field strength

$$H = \frac{N_1}{L} \cdot I_1$$

L : effective length of iron core,
 N_1 : number of windings of primary coil.

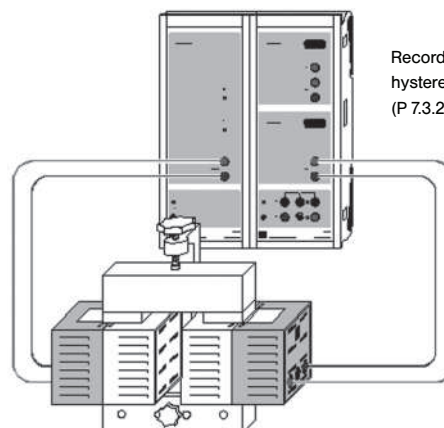
The corresponding magnetic induction value B is obtained through integration of the voltage U_2 induced in the secondary coil of a transformer:

$$B = \frac{1}{N_2 \cdot A} \cdot \int U_2 \cdot dt$$

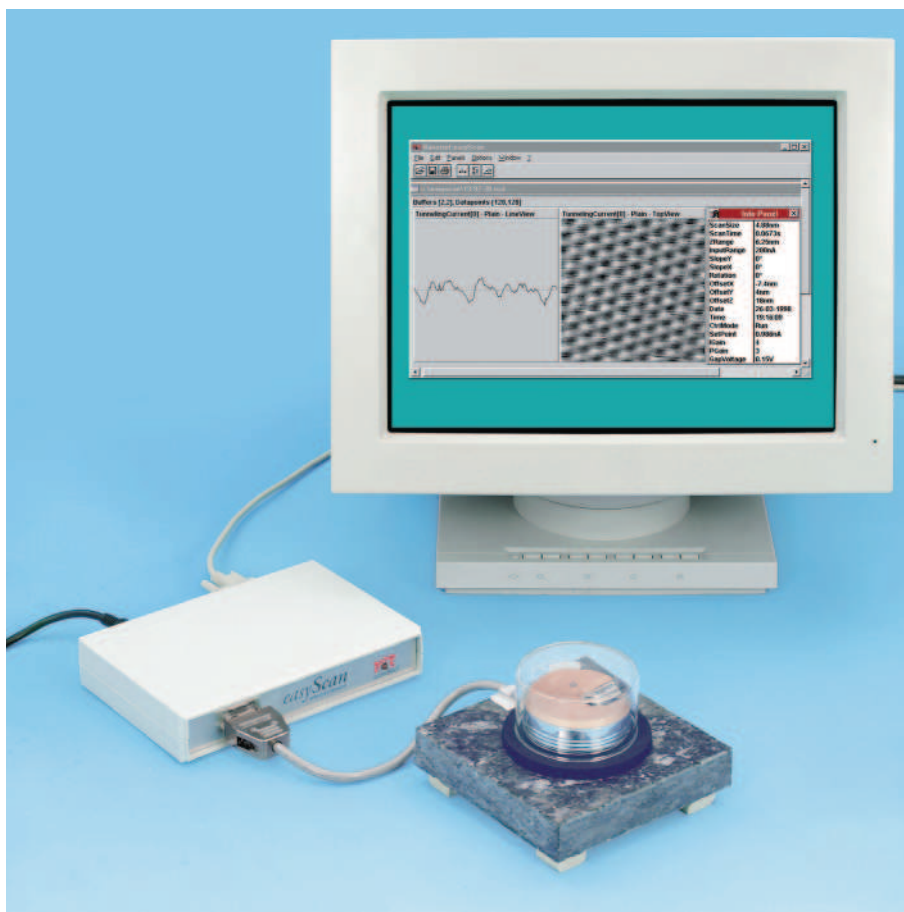
A : cross-section of iron core
 N_2 : Number of windings of secondary coil

The computer-assisted measurement system CASSY is used to control the current and to record and evaluate the measured values. The aim of the experiment is to determine the relative permeability μ_r in the magnetization curve and the hysteresis curve as a function of the magnetic field strength H .

Cat. No.	Description	P 7.3.2.1 (a)	P 7.3.2.1 (b)
562 11	U-core with yoke	1	1
562 12	Clamping device	1	1
562 14	Coil with 500 turns	2	2
522 621	Function generator S 12, 0.1 Hz to 20 kHz	1	
524 010USB	Sensor-CASSY	1	1
524 200	CASSY Lab	1	1
524 011USB	Power-CASSY		1
576 71	Rastered socket panel section	1	
577 19	STE resistor 1 Ω , 2 W	1	
500 444	Connecting lead, 100 cm, black	7	4
500 424	Connecting lead, 50 cm, black	1	
additionally required: PC with Windows 95/NT or higher		1	1



Recording the magnetization and hysteresis curves of a ferromagnet (P 7.3.2.1 b)



Investigating a graphite surface using a scanning tunneling microscope (P 7.4.1.1)

P 7.4.1**Scanning tunneling microscope**

- P 7.4.1.1 Investigating a graphite surface using a scanning tunneling microscope
- P 7.4.1.2 Investigating a gold surface using a scanning tunneling microscope
- P 7.4.1.3 Investigating a MoS₂ probe using a scanning tunneling microscope

Cat. No.	Description	P 7.4.1.1-2	P 7.4.1.3
554 581	Scanning tunneling microscope	1	1
554 584	MoS ₂ probe		1
	additionally required: PC with Windows 2000 or higher	1	1

The scanning tunneling microscope was developed in the 1980's by *G. Binnig* and *H. Rohrer*. It uses a fine metal tip as a local probe; the probe is brought so close to an electrically conductive sample that the electrons "tunnel" from the tip to the sample due to quantum-mechanical effects. When an electric field is applied between the tip and the sample, an electric current, the tunnel current, can flow. As the tunnel current varies exponentially with the distance, even an extremely minute change in distance of 0.01 nm results in a measurable change in the tunnel current. The tip is mounted on a platform which can be moved in all three spatial dimensions by means of piezoelectric control elements. The tip is scanned across the sample to measure its topography. A control circuit maintains the distance between tip and sample extremely precisely at a constant distance by maintaining a constant tunnel current value. The controlled motions performed during the scanning process are recorded and imaged using a computer. The image generated in this manner is a composite in which the sample topography and the electrical conductivity of the sample surface are superimposed.

These experiments use a scanning tunneling microscope specially developed for practical experiments, which operates at standard air pressure. At the beginning of the experiment, a measuring tip is made from platinum wire. The graphite sample is prepared by tearing off a strip of tape. When the gold sample is handled carefully, it requires no cleaning; the same is valid for the MoS₂ probe. The investigation of the samples begins with an overview scan. In the subsequent procedure, the step width of the measuring tip is reduced until the positions of the individual atoms of the sample with respect to each other are clearly visible in the image.

P 7.5.1

X-ray fluorescence analysis

P 7.5.1.1 Application of x-ray fluorescence for the non-destructive analysis of the chemical composition

P 7.5.1.2 Determination of the chemical composition of a brass sample by x-ray fluorescence analysis



Recording of X-ray fluorescence (P 7.5.1.1+2)

X-ray fluorescence is a very useful tool for a non-destructive analysis of the chemical composition of a target alloy. When irradiating a sample with x-rays, all the different elements it contains emit characteristic x-rays due to fluorescence, which are fingerprints of every single element.

In experiment P 7.5.1.1, x-ray fluorescence is used to do qualitative analysis by identifying the substances in four alloy samples, made from chrome-nickel steel, two different kinds of brass and rare earth magnet.

In experiment P 7.5.1.2, the composition of one brass alloy is analysed quantitatively. The weight percentage of each component in the alloy is calculated from the strength of different fluorescence lines.

Cat. No.	Description	P 7.5.1.1	P 7.5.1.2
554 811USB	X-ray apparatus	1	1
559 938	X-ray energy detector	1	1
554 848	Set of targets alloys	1	1
554 844	Set of targets K-line fluorescence		1
554 846	Set of targets L-line fluorescence		1
524 010USB	Sensor-CASSY	1	1
524 058	MCA Box	1	1
524 200	CASSY Lab	1	1
501 02	BNC Cable, 1 m	1	1
	additionally required: PC with Windows 98/NT or higher	1	1